Robotica: (2021) volume 39, pp. 633–651. © The Author(s), 2020. Published by Cambridge University Press.
doi:10.1017/S0263574720000636

Delayed Bilateral Teleoperation of the Speed and Turn Angle of a Bipedal Robot

Viviana Moya*, Emanuel Slawiñski and Vicente Mut

Instituto de Automática (INAUT), Universidad Nacional de San Juan, San Juan, Argentina
Emails: slawinski@inaut.unsj.edu.ar; vmut@inaut.unsj.edu.ar

(Accepted June 19, 2020. First published online: July 14, 2020)

SUMMARY
This paper proposes a shared control scheme which aims to achieve a stable control of the speed and turn of a bipedal robot during a delayed bilateral teleoperation. The strategy allows to get a delay-dependent damping value that must be injected to assure a bounded response of the hybrid system, while simultaneously, the human operator receives a force feedback that help him to decrease the synchronism error. Furthermore, a test where a human operator handles the walking of a simulated bipedal robot, to follow a curve path in front of varying time delay, is performed and analyzed.

KEYWORDS: Bilateral teleoperation; Bipedal robot; Time-varying delay; Turn; Stable walk.

1. Introduction

The humanoid robots can perform several tasks in an automatic way with diverse field applications encouraged by the technological permanent advance. To ensure that a humanoid robot will be a viable option to achieve these goals, one of the main problems concerns the capability of the robot to move from one location to another. Thus, it is important to develop schemes to ensure stable walk with forward velocity and to control the turn of the bipedal robot.[1,2] There are several ways in the literature to generate the references for each actuator,[1,3,4] even based on the observation and measurement of the standard human walk.[4] On the other hand, a relevant amount of technology has been developed to build bipedal or humanoid robots, such as the QRIO, ONDA, NAO, and ASIMO robots. Those projects had been constantly improving and adding capabilities such as the ability to evade obstacles by turning around them and follow various curve paths in many directions with the ability to move forward, backward, left, right, or even up and down stairs on even and uneven terrains.[2] Most papers presented in the state of the art are based on the use of the zero-moment point (ZMP) criterion, which states that the stability of the robot is conditioned by the existence of the ZMP within the support polygon of the robot.[1] ZMP refers to a point on the ground on which the horizontal component of the movement resulting from the ground reaction force is zero. Besides, artificial intelligence methods, as the one in ref. [5], are also used, where an adaptive neural-fuzzy walking control of an autonomous biped is proposed, using a prefeeding neural network based on linear regression to build the controller. In ref. [6], a zero-moment trajectory generator with neuronal-fuzzy that reduces the movement of the trunk and therefore significantly improve the stability of the bipedal robot walk is proposed. On the other hand, in truly dynamic methods, the hypothetical ZMP may be outside the support polygon and even then, the biped does not experience instability. The strict conditions of the use of ZMP limit the speed that can be achieved and result in an inefficient passage cycle. A different philosophy, called the hybrid zero dynamics (HZD) method,[1,4] has been proposed to generate periodic dynamic walks for underactuated bipeds; the purpose of this method is to reduce the size of the system and facilitate stability analysis. In this method, input–output linearization is implemented to design a controller that produces a walking step when zeroing a set of appropriate outputs designed as virtual holonomic constraints. In order to ensure a proper turn control of the

* Corresponding author. E-mail: vmoya@inaut.unsj.edu.ar

humanoid robot, a diverse set of methods have been studied, such as the HZD, this method has been used to stabilize periodic gaits for 3D bipeds[7] and to steer the robot along paths with mild curvature following a single predefined periodic motion.[2] There are other techniques like geometric reduction and passivity-based control to stable walking and steering of fully actuated 3D robots,[8,9] turning motion of a bipedal robot by slipping the feet on the ground,[10] and using policy gradient method. This last method has many advantages including smooth walking patterns and modulation during walking to increase or decrease its speed,[11] among others.

On the other hand, robot teleoperation allows to extend and transport the capabilities and skills of a human operator toward remote work environments. In these systems, a human operator located at a local site sends speed or position commands to a robot that is navigating in a distant environment, which could be dangerous, harmful, and perhaps physically inaccessible for a human operator. In addition, both sites are connected through a communication channel such as the Internet that adds time-varying delays that could decrease the performance and transparency of the system.[12] Regarding teleoperation of bipedal and/or humanoid robots, ref. [13] uses the human sensorimotor learning ability to teach a humanoid robot how to compliantly interact with the environment, in ref. [14], an operator was fed back with force signals informing him of the position of the ZMP within the humanoid support polygon, this measurement was used to give the operator an idea of the balance of the robot using a vibrotactile belt for providing cutaneous haptic balance feedback. During the tests performed, the operator is informed trough haptic signals coming from the vibrotactile belt about the stability while commanding the humanoid's hands, and in ref. [15], a balance feedback interface is introduced using a kinesthetic system that applies forces to the operator's waist to inform him of his proximity to the edges of the support polygon. Also there are many strategies based on the use of motion capture devices such as the Kinect in order to map the movements of a human operator to the robot,[16,17] but this case is nonbilateral, that is, without force feedback.

To the best knowledge of the authors, there are not proposals in the state of the art addressed to the bilateral teleoperation of bipedal robots that consider time-varying delays. In this paper, we present a control scheme addressed to delayed bilateral teleoperation of the forward velocity and turn of a bipedal robot keeping a stable walking. A shared control strategy is proposed where some degrees of freedom are teleoperated and other automatically controlled. The proposed strategy links a bilateral controller for teleoperation, a walking control scheme for handling the forward velocity and turning angle, and an automatic control for the lateral (roll) and frontal (pitch) equilibriums through the torso pose. The bipedal robot is modeled by a hybrid dynamic system and it is linked with the theory of delayed bilateral teleoperation (delayed nonlinear continuous systems) via a continuous virtual slave, which is coupled with the bipedal robot through a spring-damper link impedance. Furthermore, human-inspired references are applied based on common human foot trajectories in cartesian coordinates, modulated by the hip velocity reference, and the turn references are based on partial hybrid zero dynamics (PHZD). As result to apply this proposal, we get a delay-dependent condition for the damping that must be injected into the master and bipedal robot to assure a bounded response of the hybrid system, while simultaneously the human operator receives a force feedback that cause slower motions of the master as the time delay is higher and impulsing the human operator hand to directions of lower errors between the master position and the velocity and turn angle of the bipedal slave. Besides, a test of bilateral teleoperation of an NAO robot simulated in VREP, including time-varying delay, is performed. This paper is organized as follows: Section 2 presents the preliminaries and models used, describing the hybrid model of a bipedal robot. In Section 3, a novel controller for delayed bilateral teleoperation of a bipedal robot is proposed, and its stability is analyzed in Section 4. Then, Section 5 shows the results achieved where a human operator drives a 3D bipedal robot-like NAO using the V-REP simulation environment. Finally, conclusions are exposed in Section 6.

2. Preliminaries

In this section, we present the mathematical tools that are used in this paper as the mathematical models for the devices that are used to describe the model of the master and the slave to perform teleoperation control.

2.1. Mathematical preliminaries

To clarify the mathematic procedure exposed in the next sections, the main notation is described below. If x is a scalar, $\mathbf{w}$ is a vector, and $\mathbf{Y}$ is a matrix, then $|x|$ is the absolute value of x,$|\mathbf{w}|$ is a vector

https://doi.org/10.1017/S0263574720000636 Published online by Cambridge University Press

Table I. Nomenclature.

Variable	Definition
$\mathbf{x_m} = \left[x_{mv}\ x_{m\delta}\right]^T$	Master position
v	Virtual linear velocity
v_{hip}	Bipedal linear velocity
δ	Virtual turn angle
δ_{NAO}	Bipedal turn angle
$\mathbf{f_s}$	Force and torque applied to the virtual slave
$\mathbf{f_v}$	External virtual force
$\mathbf{f_m}$	Force applied to the master device
$\tilde{y}_1$	Linear velocity error
$\tilde{\mathbf{y}}_\mathbf{2}$	Joints velocity error
$\tilde{y}_3$	Turn angle error

where each component is the value absolute of each component of the vector $\mathbf{w}$, $\|\mathbf{x}\|$ is the Euclidean norm of $\mathbf{x}$, $\mathbf{Y} > 0 (\mathbf{Y} < 0)$ means that $\mathbf{Y}$ is positive definite (negative definite). In addition, $\|\mathbf{w}\|_2$ and $\|\mathbf{w}\|_\infty$ represent the $\mathcal{L}_2$-norm and $\mathcal{L}_\infty$- norm of $\mathbf{w}$, respectively. Table I shows the nomenclature used in this paper.

Lemma 1. (Ref. [18]) For vector functions $\mathbf{a}(.)$ and $\mathbf{b}(.)$ and a time-varying scalar $h(t)$ with $0 \leq h(t) \leq \bar{h}$, the following inequality holds:

$$\begin{aligned} -2\mathbf{a}^T(t) \int_{t-h(t)}^{t} \mathbf{b}(\xi) d\xi - \int_{t-h(t)}^{t} \mathbf{b}^T(\xi)\mathbf{b}(\xi)\, d\xi &\leq h(t)\, \mathbf{a}^T(t)\, \mathbf{a}(t), \\ &\leq \bar{h}(t)\, \mathbf{a}^T(t)\, \mathbf{a}(t). \end{aligned} \tag{1}$$

Definition 1. (Ref. [19]) For the system,

$$\dot{\mathbf{x}} = f(\mathbf{x}, z) + g(\mathbf{x}, z)\mathbf{u}_\epsilon(\mathbf{x}, z), \tag{2}$$

a parameter family of continuously differentiable functions $V_\epsilon : X \to \mathbb{R}$ is said to be a rapidly exponentially stabilizing control Lyapunov function, if there exist positive constants $c_1, c_2, c_3 > 0$ that for all, $(\mathbf{x}, z) \in X \times Z$, hold the following conditions:

$$c_1\|\mathbf{x}\|^2 \leq V_\epsilon(\mathbf{x}) \leq c_2\|\mathbf{x}\|^2, \tag{3}$$

$$\inf_{u \in U}\left[L_f V_\epsilon(\mathbf{x}, z) + L_g V_\epsilon(\mathbf{x}, z)\mathbf{u}_\epsilon + c_3 V_\epsilon(\mathbf{x})\right] \leq 0, \tag{4}$$

where the controller becomes to:

$$K_\epsilon(\mathbf{x}, z) = \left\{\mathbf{u}_\epsilon \in U : L_f V_\epsilon(\mathbf{x}, z) + L_g V_\epsilon(\mathbf{x}, z)\mathbf{u}_\epsilon + c_3 V_\epsilon(\mathbf{x}) \leq 0\right\}. \tag{5}$$

Consisting of the control actions that result in $\dot{V}_\epsilon(\mathbf{x}, z, \mathbf{u}_\epsilon) \leq -c_3 V_\epsilon(\mathbf{x})$. For any Lipschitz continuous feedback control law $\mathbf{u}_\epsilon(\mathbf{x}, z) \in K_\epsilon$, the solutions of the close-loop system satisfy an exponential response given by:

$$V_\epsilon(\mathbf{x(t)}) \leq e^{-c_3 t} V_\epsilon(\mathbf{x(0)}), \tag{6}$$

$$\|\mathbf{x(t)}\| < \sqrt{\frac{c_2}{c_1}} e^{-c_3 t}\|\mathbf{x(0)}\|. \tag{7}$$

2.2. Models of master and virtual slave

The master can have serial- or parallel-type configuration. In the paper, a Novint Falcon is used, which has a kinematics model described in ref. [20], and this model can be represented in the task space as follows:

$$\mathbf{M_m}(\mathbf{x_m})\ddot{\mathbf{x}}_\mathbf{m} + \mathbf{C_m}(\mathbf{x_m}, \dot{\mathbf{x}}_\mathbf{m})\dot{\mathbf{x}}_\mathbf{m} + \mathbf{g_m}(\mathbf{x_m}) = \mathbf{f_m} + \mathbf{f_h}, \tag{8}$$

https://doi.org/10.1017/S0263574720000636 Published online by Cambridge University Press

The Novint Falcon haptic device has three degrees of freedom, where two of them are used to teleoperate a bipedal robot, and the third degree of freedom is not used but a gravity compensation was applied. Furthermore, $\mathbf{x_m} = \left[x_{mv}\ x_{m\delta}\right]^T \in R^{n\times 1}$ and $\dot{\mathbf{x}}_\mathbf{m}$ are the master position and velocity, $\mathbf{M_m}\ (\mathbf{x_m}) \in R^{n\times n}$ is the inertia matrix, $\mathbf{C_m}\ (\mathbf{x_m}, \dot{\mathbf{x}}_\mathbf{m})$ is the matrix representing centripetal and Coriolis forces, $\mathbf{g_m}\ (\mathbf{x_m})$ is the gravitational force, $\mathbf{f_h}$ is the force caused by the human operator, and $\mathbf{f_m}$ is the control force applied to the master which will be computed by the controller.

For the remote virtual robot, the following 2D virtual dynamic model to represent their linear velocity and turn angle is used:

$$\mathbf{D}\dot{\boldsymbol{\eta}} = \mathbf{f_s} - \mathbf{f_v}, \tag{9}$$

where $\boldsymbol{\eta} = \left[v\ \delta\right]^T$ is a vector that link the linear virtual velocity of the robot represented with v and the turn angle of the virtual slave represented with δ, $\mathbf{D}$ is the mass of the virtual robot, the control action $\mathbf{f_s}$ involves a force and torque applied to the virtual robot, and $\mathbf{f_v}$ is the external virtual force that holds $\mathbf{f_v} \in \mathcal{L}_\infty \cap \mathcal{L}_2$ with $\|\mathbf{f_v}\| \leq \bar{f}_v$ (positive constant).

2.3. Assumptions and properties

The following ordinary properties and assumptions will be used in this paper:[18,21]

Property 1. The inertia matrices $\mathbf{M_m}\ (\mathbf{x_m})$ and $\mathbf{D}$ are symmetric positive defined.

Property 2. The matrix $\dot{\mathbf{M}}_\mathbf{m}\ (\mathbf{x_m}) - 2\mathbf{C_m}\ (\mathbf{x_m}, \dot{\mathbf{x}}_\mathbf{m})$ is skew-symmetric, that is, $\dot{\mathbf{M}}_\mathbf{m}\ (\mathbf{x_m}) = \mathbf{C_m}\ (\mathbf{x_m}, \dot{\mathbf{x}}_\mathbf{m}) + \mathbf{C}_\mathbf{m}^\mathbf{T}\ (\mathbf{x_m}, \dot{\mathbf{x}}_\mathbf{m})$.

Property 3. For all $\dot{\mathbf{x}}_\mathbf{m}, \ddot{\mathbf{x}}_\mathbf{m} \in R$, there exists a $\kappa_m, \kappa_s > 0$ such that $\mathbf{C_m}\ (\mathbf{x_m}, \dot{\mathbf{x}}_\mathbf{m})\ \dot{\mathbf{x}}_\mathbf{m} \leq \kappa_m\ |\dot{\mathbf{x}}_\mathbf{m}|$ for all time t.

Property 4. If $\dot{\mathbf{x}}_\mathbf{m}, \ddot{\mathbf{x}}_\mathbf{m}$ are bounded, then $\dot{\mathbf{C}}_\mathbf{m}$ is bounded.

Assumption 1. The communication channel adds a forward time delay h_1(from the master to the slave) and a backward time delay h_2 (from the slave to the master). These delays are time varying, bounded, and asymmetric. Therefore, there exist positive values $\bar{h}_1$ and $\bar{h}_2$ such that $0 \leq h_1\ (t) \leq \bar{h}_1$ and $0 \leq h_2\ (t) \leq \bar{h}_2$ for all t.

Assumption 2. The user is represented by a damping-like model plus a nonmodeled signal of finite energy, or with a simplification of it[22]:

$$\mathbf{f_h} = -\alpha_h \dot{\mathbf{x}}_\mathbf{m} + \mathbf{f_{a_h}}, \tag{10}$$

where $\alpha_h > 0$ is the damping-like intrinsic parameter of the human operator, and $\mathbf{f_{a_h}} \in \mathcal{L}_\infty \cap \mathcal{L}_2$ and holds $\left\|\mathbf{f_{a_h}}\right\| \leq \bar{f}_{a_h}$ with $\left\|\dot{\mathbf{f}}_{\mathbf{a_h}}\right\|$ bounded,where $\bar{f}_{a_h}$ is a positive constant value.

2.4. Model of bipedal robot

A bipedal robot can be modeled in a simplified way on a sagittal plane (longitudinal plane that divides the body into left and right) for walk references while the turn is included using the hip's yaw angles of the 3D bipedal robot, taking into consideration the invariance property in front of yaw rotations.[2] The robot used in this work is the NAO that includes a torso, hip, and two identical legs with knees and ankles. When only one leg is in contact with the ground, the contacting leg is known as the stance leg and other is known as the swing leg. Then, when a foot is on the ground it is defined as the single or swing phase. On the contrary, when both feet are on the ground, it is known as a double-support phase.[1] The presence of impacts and the variant nature of the contact conditions at the end of the legs with the environment during the walking cycle (due to the torque and lifting of the foot and possibly the heel strike and rotation) necessarily generate models that have multiple phases, and therefore they are hybrids. So that a hybrid system representing a bipedal robot involves a behavior continuous (when the leg moves forward) and discrete (when the foot touches the ground which generates impulsive responses).[1]

The bipedal robot's continuous dynamics between successive impacts is modeled in a similar way to two robotic manipulators with $n = 4$ actuators for each leg. The bipedal robot state is featured by $\mathbf{x} = \left[\mathbf{q}\ \dot{\mathbf{q}}\right]^T$ its position $\mathbf{q} \in R^{2n}$ and velocity $\dot{\mathbf{q}} \in R^{2n}$ which is represented by the following state-space model:

https://doi.org/10.1017/S0263574720000636 Published online by Cambridge University Press

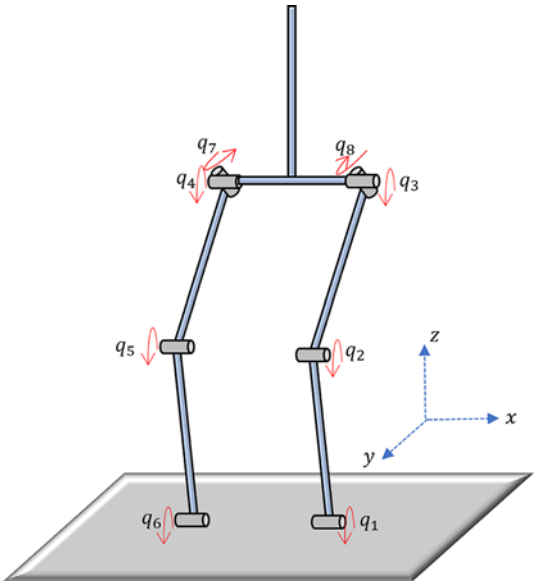

Fig. 1. Location of the angles in a bipedal robot.

$$\begin{aligned} \begin{bmatrix} \dot{\mathbf{q}} \\ \ddot{\mathbf{q}} \end{bmatrix} &= f(\mathbf{q}, \dot{\mathbf{q}}) + g(\mathbf{q})\,\mathbf{u}_{\epsilon}, \\ f(\mathbf{q}, \dot{\mathbf{q}}) &= \begin{bmatrix} \dot{\mathbf{q}} \\ -\mathbf{M}^{-1}(\mathbf{q})\left[\mathbf{C}(\mathbf{q}, \dot{\mathbf{q}}) + \mathbf{G}(\mathbf{q})\right] \end{bmatrix}, \; g(\mathbf{q}) = \begin{bmatrix} 0 \\ \mathbf{M}^{-1}(\mathbf{q})\mathbf{B}(\mathbf{q}) \end{bmatrix}, \end{aligned} \tag{11}$$

where $\mathbf{M}$ represents the inertia matrix, $\mathbf{C}$ represents the Coriolis and centripetal torques, $\mathbf{G}$ is the gravity vector, and $\mathbf{B}$ is the input matrix. In addition, it is defined: $\mathbf{q} = \begin{bmatrix} q_1 & q_2 & q_3 & q_4 & q_5 & q_6 & q_7 & q_8 \end{bmatrix}^T$ and $\mathbf{u}_{\epsilon} = \begin{bmatrix} u_1 & u_2 & u_3 & u_4 & u_5 & u_6 & u_7 & u_8 \end{bmatrix}^T$, where the $u_i = 1, \ldots, 8$ torques are applied to the left ankle whose pitch angle is q_1, the left knee's pitch angle q_2, the left hip's pitch angle q_3, the right hip's pitch angle q_4, the right knee's pitch angle q_5, the right ankle's pitch angle q_6, the right hip's yaw angle q_7, and the left hip's yaw angle q_8, respectively, as shown in Fig. 1.

It is important to remark that a stable continuous dynamic does not ensure a stable dynamic of the hybrid system. When an impact is produced between one or both legs and the floor, an environment force appears modeled like an impulse, changing the joint's velocities instantly. Hybrid systems are also known as systems with impulsive effects, and in general they can be used to model a bipedal robot. In addition, we assume that there exists a hybrid dynamics represented by:[1,19]

$$W_{\varepsilon} = \begin{cases} \dot{\mathbf{x}} = f(\mathbf{x}, z) + g(\mathbf{x}, z)\,\mathbf{u}_{\varepsilon}(\mathbf{x}, z) & if\ (\mathbf{x}, z) \in D \setminus S \\ \dot{z} = w(\mathbf{x}, z) & \\ \mathbf{x}^{+} = \Delta_X\left(\mathbf{x}^{-}, z^{-}\right) & if\ \left(\mathbf{x}^{-}, z^{-}\right) \in S \\ z^{+} = \Delta_Z\left(\mathbf{x}^{-}, z^{-}\right) & \end{cases}, \tag{12}$$

where $\mathbf{x} \in X$, $z \in Z$ represents the hip velocity that depends on the joint velocities and $z^{+} := (x^{+}; z^{+})$ (resp. $z^{-} := (x^{-}; z^{-})$) is the state value just after (resp. just before) impact, D is a sub-space of R^{4n+1} defined as $D = \left\{\left[\mathbf{x}\ z\right] \in R^{4n+1} : l(\mathbf{q}) \geq 0\right\}$, $S \subset D$ is an proper sub-set of D called switching surface, defined by $S = \left\{\left[\mathbf{x}\ z\right] \in R^{4n+1} : l(\mathbf{q}) = 0,\ dl(\mathbf{q})\,\dot{\mathbf{q}} < 0\right\}$, with l as the height of the oscillating foot respect to the floor in cartesian coordinates and $dl(\mathbf{q})$ is the partial derivate of l respect to $\mathbf{q}$, and $U \subseteq R^{2n+1}$ is the control's action set with $\mathbf{u}_{\epsilon} \in K_{\epsilon}$ (Definition 1). Besides, $\Delta_X : S \to D$ is a mapping that produces a switching between the stand and oscillation legs changing the impact angles accordingly, while Δ_Z determines how velocity changes according to the foot-floor impact front.

For the hybrid system, let $\phi_t^{\epsilon}(t, [\mathbf{x}, z])$ be a flow of the continuous dynamics of (12) then for $(\mathbf{x}^*, z^*) \in S$, ϕ_t^{ϵ} is a hybrid periodic response with period $T > 0$ if $\phi_t^{\epsilon}(T, [\Delta_X(\mathbf{x}^*, z^*), \Delta_Z(\mathbf{x}^*, z^*)]) = (\mathbf{x}^*, z^*)$. O is a hybrid periodic orbit if $O = \left\{\phi_t^{\epsilon}(t, [\Delta_X(\mathbf{x}^*, z^*), \Delta_Z(\mathbf{x}^*, z^*)]) : 0 \leq t \leq T\right\}$ for a

https://doi.org/10.1017/S0263574720000636 Published online by Cambridge University Press

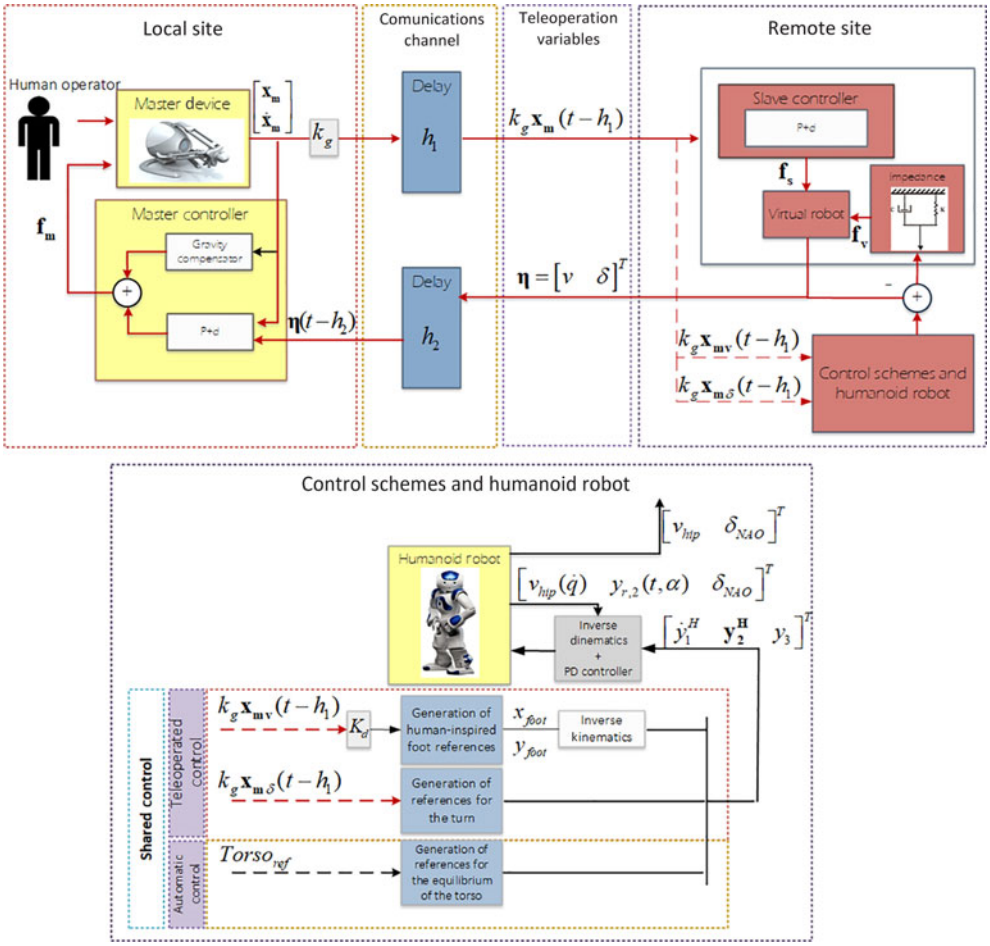

Fig. 2. Proposed shared control scheme for delayed bilateral teleoperation of a bipedal robot.

periodic solution ϕ_t^ϵ. Besides, a Poincaré map $P^\epsilon : S \to S$ is defined in ref. [19] by $P^\epsilon(\mathbf{x}, z) = \phi\left(T_I^\epsilon(\mathbf{x}, z), [\Delta_X(\mathbf{x}, z), \Delta_Z(\mathbf{x}, z)]\right)$, where $T_I^\epsilon(\mathbf{x}, z) = \inf\left\{t \geq 0 : \phi_t^\epsilon(t, [\Delta_X(\mathbf{x}, z), \Delta_Z(\mathbf{x}, z)]) \in S\right\}$ is the time-to-impact function, as in refs. [4, 19]. The Poincaré map is locally exponentially stable (as a discrete time system) at fixed point $(\mathbf{x}^*, z^*)$ if and only if the periodic orbit O is locally exponentially stable.[4]

3. Controller for Delayed Bilateral Teleoperation of Bipedal Robot

The presented control scheme allows to bilaterally teleoperate the speed and turn angle of a bipedal robot, where the torso pose is autonomously controlled to reach adequate lateral and frontal equilibrium. Figure 2 shows the proposed shared control scheme whose main parts are the following:

- Bilateral controller for teleoperation, where the response of the bipedal robot must be bounded by the evolution of a virtual continuous slave which is coupled to the bipedal robot one via an elastic-damper system.
- Walking control scheme to drive the forward velocity, where the references for the knee and hip are human inspired considering a constant walking cycle time, based on an analysis of a foot in a common human walk in cartesian coordinates.
- Turning angle control, where the references are set based on the invariance property in front of yaw rotations and hold a condition based on PHZD concept.
- Automatic control for the lateral (roll) and frontal (pitch) equilibriums through the torso pose is necessary to have a stable walking.
- Controller based on inverse dynamics that allow linearize and decouple the bipedal robot.

https://doi.org/10.1017/S0263574720000636 Published online by Cambridge University Press

Additionally, the human operator simultaneously receives force feedback that improves the perception to teleoperate the bipedal robot, preventing rapid movements of the master, depending on the time delay, as well as pushing the human operator hand to directions of lower errors between the master and bipedal robot.

3.1. P+d external controller

In this section, a controller for bilateral teleoperation of a bipedal robot is proposed and its stability is analyzed considering the time delays added by the communication channel. As described in the literature, the P+d controllers are simple and robust structures that work well for several applications including bilateral teleoperation systems of manipulator robots[21,23] and bilateral teleoperation of mobile robots[24,25] where a sufficiently high value of damping is injected to assure stability. The following equations are based on the bilateral teleoperation of mobile robots,[24] extended to bipedal robots by using a spring-damper like impedance (16) to couple the bipedal robot with a virtual slave depending on the difference between the bipedal robot velocity and the virtual slave velocity:

$$\mathbf{f_m} = -k_m \left(k_g \mathbf{x_m} - \boldsymbol{\eta}\,(t-h_2)\right) + \mathbf{g_m}\,(\mathbf{x_m}) - \alpha_m \dot{\mathbf{x}}_m, \tag{13}$$

$$\mathbf{f_s} = k_s \left(k_g \mathbf{x_m}\,(t-h_1) - \boldsymbol{\eta}\right) - \sigma_s \boldsymbol{\Psi}, \tag{14}$$

$$\boldsymbol{\Psi} = \dot{\boldsymbol{\eta}}(t-\gamma), \tag{15}$$

$$\mathbf{f_v} = \boldsymbol{\Omega}\,(\cdot)\,\bar{f}_v \tanh\left(\frac{1}{\bar{f}_v}\left[\beta_1\left(v_{hip} - \boldsymbol{\eta}\right) + \beta_2\left(\dot{v}_{hip} - \boldsymbol{\Psi}\right)\right]\right). \tag{16}$$

The control parameters have positive values, where k_s and k_m represent positive constant gain values, k_g linearly maps the master position to a speed and turn angle references of a virtual robot represented by the $\boldsymbol{\eta} = \left[v\ \delta\right]^T$, where v and δ are the speed and turn angle of the virtual bipedal robot, α_m and σ_s are coefficients of damping injected in the real master and virtual robot, v_{hip} represents the hip velocity of the bipedal robot, β_1 is the elasticity coefficient, and β_2 is the damping coefficient of the coupling impedance. The function $\boldsymbol{\Omega}\,(\cdot)$ have a bounded output that tends to zero for $t \to \infty$ in order to assure that $\mathbf{f_v} \in L_2$. On the other hand, the signal $\boldsymbol{\Psi}$ represents the linear acceleration and the angular velocity of virtual robot at an infinitesimal time $\gamma \to 0^+$ before t. Due to these signals are from a virtual slave and not from a real system, such signals are available. In addition, in ref. [26], a state variable observer is applied to avoid using acceleration measures which are generally noisy.

3.2. Generation of references

In the proposed scheme, some of the generated signals are teleoperated, while others have been controlled automatically. All references used in the development of the control scheme for forward velocity of the bipedal robot are human inspired and have been established through the study of the walking patterns of test subjects, observing the foot trajectory in cartesian coordinates to track their movement across the floor while walking. Meanwhile, the references for the turn are based on a PHZD.

Focusing first on the references for forward velocity, according to ref. [27], each limb consumes approximately 40% of the cycle as a single support leg, 20% as part of the double support, and 40% as a swinging leg. Once the foot trajectory data have been analyzed, human-inspired references are obtained by using an approximation by a Bezier curve (17) plus a straight line. Such Bezier function depends on coefficients $\boldsymbol{\alpha} = \left[\alpha_1\ \alpha_2\ \alpha_3\ \alpha_4\right]$ that featured a Bezier curve of order 3, where these coefficients dependent on the speed reference. The Bezier function is defined by:

$$\begin{aligned}&\left[x_{foot}\left(v_{ref}, \boldsymbol{\alpha}, t_{bezier}\right), y_{foot}\left(v_{ref}, \boldsymbol{\alpha}, t_{bezier}\right)\right] := \\ &\sum_{i=0}^{3} \binom{3}{i} (1 - t_{bezier})^{3-i}\, {t_{bezier}}^i \boldsymbol{\alpha},\ i = 0, \ldots 3,\end{aligned} \tag{17}$$

where $t_{bezier} = [0, 1]$ goes from 0 to 1. The $\boldsymbol{\alpha}$ parameters are found by optimization to ensure that the trajectory of the robot foot be as close as possible to the typical trajectory of a person (scaled to the size of the robot used), this is the following cost function P is minimized respect to the $\boldsymbol{\alpha}$.

https://doi.org/10.1017/S0263574720000636 Published online by Cambridge University Press

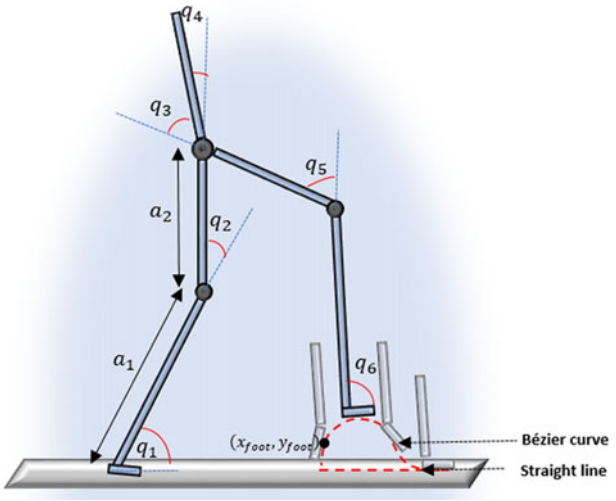

Fig. 3. Foot path and joint angles of the bipedal robot.

$$P(\boldsymbol{\alpha}) = \int_0^T \left(x_{foot}\left(v_{ref}, \boldsymbol{\alpha}, t_{bezier}\right) - X_{ref}\left(t_{bezier}\right)\right)^2 dt + \int_0^T \left(y_{foot}\left(v_{ref}, \boldsymbol{\alpha}, t_{bezier}\right) - Y_{ref}\left(t_{bezier}\right)\right)^2 dt, \tag{18}$$

where $X_{ref}(t)$ and $Y_{ref}(t)$ are the human-inspired waveforms obtained from ref. [28], which are parameterized for $t = [0, 0.4T]$, while the straight line is act due in the range $[0.4T, T]$. Next, to obtain the join references from the generated cartesian trajectory, inverse kinematics[29] is applied to get the angles of knee and hip during a walk cycle of period T, see Fig. 3, as follows:

$$q_2 = a\tan 2\left(y_{foot}, x_{foot}\right) - \cos^{-1}\left(\frac{a_1^2 + x_{foot}^2 + y_{foot}^2 - a_2^2}{2a_1\sqrt{x_{foot}^2 + y_{foot}^2}}\right), \tag{19}$$

$$q_3 = \cos^{-1}\left(\frac{x_{foot}^2 + y_{foot}^2 - a_1^2 - a_2^2}{2a_1a_2}\right), \tag{20}$$

where a_1, a_2 are leg link lengths, as shown in Fig. 3.

Taking into account the percentages with respect to T of the support and double phase and considering that the legs are symmetrical, angles q_4 and q_5 are calculated using a phase shift of the angles q_2 and q_3, while the ankle's angles q_1 and q_6 are provided indirectly from the hip's velocity for both legs, as it will be described in Section 3.3.

Finally, the references $\mathbf{Y} = \left[\dot{y}_1^H \ \mathbf{y_2^H} \ y_3\right]$ are defined by:

$$\dot{y}_1^H(\boldsymbol{\alpha}) = k_g x_{mv}\left(t - h_1\right) = v_{ref}, \tag{21}$$

$$\mathbf{y_2^H}\left(t, v_{ref}\right) = \left[q_1\left(t, v_{ref}\right)\ q_2\left(t, v_{ref}\right)\ q_3\left(t, v_{ref}\right)\ q_4\left(t, v_{ref}\right)\right]^T, \tag{22}$$

$$y_3(t) = f\left(k_g x_{m\delta}\left(t - h_1\right)\right) = \delta_{ref}(t), \tag{23}$$

where v_{ref} is the hip velocity reference and $\delta_{ref}(t)$ is the relative turn angle reference of the bipedal robot, which is online computed by the following proposed equations:

$$\triangle(t) = \begin{cases} 0 & k_cT \le t \le 0.4T + k_cT \\ k_g x_{m\delta}\left(t + 0.4T + k_cT + kT_{turn}\right) = & \\ \quad k_g x_{m\delta}\left(0.4T + k_cT + kT_{turn}\right) & 0.4T + k_cT < t < T + k_cT \end{cases} \tag{24}$$

$$\delta_{ref}(t) = \int_0^t \left(\triangle\left(t - h_1(t)\right) - \delta_{ref}\left(t - \xi\right)\right) dt,$$

https://doi.org/10.1017/S0263574720000636 Published online by Cambridge University Press

where $\xi \to 0$, $T_{turn} = 150$[ms], $k = 0, 1, .. \frac{0.6T}{T_{turn}} - 1$ being reset in each change of $k_c = 0, 1, 2, 3...$, and $\delta_{ref}(t)$ is obtained filtering the signal $\triangle(t)$ to avoid abrupt changes of the reference.

3.3. Walk and turn control

To get the hip velocity, a linearization-based procedure used in ref. [4] is applied, where the hip's position depends on the stand foot's angle q_{sf} and stand leg's knee angle q_{sk}, and its derivative is computed by:

$$v_{hip}\left(\dot{\mathbf{q}}\right) = a_1\left(-\dot{q}_{sf}\right) + a_2\left(-\dot{q}_{sf} - \dot{q}_{sk}\right). \tag{25}$$

The stand foot's angle q_{sf} and the stand knee's angle q_{sk} are related alternately with $(\dot{q}_1, \dot{q}_2)$ or $(\dot{q}_6, \dot{q}_5)$ depending on the walk stage (double support, single support – right foot, double support, single support – left foot). Because (q_2, q_5) are established by the inverse kinematics (19), then (q_1, q_6) depends indirectly of hip velocity reference.

The relative turn angle with respect to the angle of the last cycle has been obtained by using:

$$\delta_{NAO}(t) = Turn_{NAO}(t) - Turn_{NAO}((k_c - 1)T), \tag{26}$$

where $Turn_{NAO}$ is the current turn of the bipedal robot, and $(k_c - 1)T$ is the time instant corresponding to the last start of walking cycle.

The goal is to drive the outputs of the robot in order to hold the proposed references for teleoperation, this is,

$$\dot{\tilde{y}}_1\left(\dot{\mathbf{q}}\right) = v_{hip}\left(\dot{\mathbf{q}}\right) - \dot{y}_1^H\left(\boldsymbol{\alpha}\right), \tag{27}$$

$$\tilde{\mathbf{y}}_\mathbf{2}\left(\mathbf{q}\right) = \mathbf{y}_{\mathbf{r},\mathbf{2}}\left(t, \boldsymbol{\alpha}\right) - \mathbf{y}_\mathbf{2}^\mathbf{H}\left(t, v_{ref}\right), \tag{28}$$

$$\tilde{y}_3 = \delta_{NAO} - y_3. \tag{29}$$

The dynamics of $\tilde{\mathbf{y}} = \left[\int \dot{\tilde{y}}_1\ \tilde{\mathbf{y}}_\mathbf{2}\ \tilde{y}_3\right]$ depends on $(\mathbf{x}, z)$, and it can be represented in general form using the Lie derivative notation as follows:

$$\ddot{\tilde{\mathbf{y}}}\left(\mathbf{x}, z\right) = L_f^2\tilde{\mathbf{y}}\left(\mathbf{x}, z\right) + L_g L_f\tilde{\mathbf{y}}\left(\mathbf{x}, z\right) u_\varepsilon\left(\mathbf{x}, z\right). \tag{30}$$

Now, the feedback linearization controller based on ref. [4] is stated as:

$$\mathbf{u}_\varepsilon\left(\mathbf{x}, z\right) = -L_g L_f\tilde{\mathbf{y}}\left(\mathbf{x}, z\right)^{-1}\left(L_f^2\tilde{\mathbf{y}}\left(\mathbf{x}, z\right) + \begin{bmatrix} k_s\dot{\tilde{y}}_1\left(\dot{\mathbf{q}}\right) + \sigma_{real}\dot{v}_{hip} + \dot{v}_{ref} \\ 2\varepsilon_2\dot{\tilde{\mathbf{y}}}_2 + \varepsilon_2^2\tilde{\mathbf{y}}_2 \\ k\tilde{y}_3 + \tau\dot{\delta}_{NAO} + \ddot{\delta}_{ref} \end{bmatrix}\right), \tag{31}$$

where σ_{real} and τ are the injected damping, k and k_s are a proportional gain, and $\epsilon_2 > 0$ where ϵ_2 is a control gain. If (31) is applied into (30), the following continuous dynamics is obtained:

$$\dot{v}_{hip} = -\frac{k_s}{1 + \sigma_{real}}\dot{\tilde{y}}_1, \tag{32}$$

$$\ddot{\tilde{\mathbf{y}}}_2 = -2\varepsilon_2\dot{\tilde{\mathbf{y}}}_2 - \varepsilon_2^2\tilde{\mathbf{y}}_2, \tag{33}$$

$$\dot{\delta}_{NAO} = -\frac{k}{1 + \tau}\tilde{y}_3. \tag{34}$$

As a result of the closed-loop control, the vector $\tilde{\mathbf{y}}_\mathbf{2}$ does not depend on z (hip velocity), and it is automatically driven as it is described in ref. [19], where $\tilde{\mathbf{y}}_\mathbf{2} \to 0$ exponentially at a rate of ϵ_2. Besides by ref. [2] states that small changes in desired rotation δ_{ref} will not destabilize the robot, and if the commanded rotation settles to a constant value, the robot will asymptotically tend to a new heading corresponding to the rotation reference.

https://doi.org/10.1017/S0263574720000636 Published online by Cambridge University Press

3.4. Partial hybrid zero dynamics

The use of PHZD assumes that $\tilde{\mathbf{y}}_{\mathbf{2}}$ remains invariant despite impact, while the hip velocity $\tilde{y}_1$ changes, thus in ref. [4], partial zero dynamic surface is defined by:

$$PZ_1 = \left\{ (\mathbf{x}, z) \in R^{4n+1} : \tilde{\mathbf{y}}_{\mathbf{2}}(\mathbf{q}) = \mathbf{0}, \dot{\tilde{\mathbf{y}}}_{\mathbf{2}} = \mathbf{0} \right\}. \tag{35}$$

The condition $\dot{\tilde{\mathbf{y}}}_{\mathbf{2}} = \mathbf{0}$ is held because the foot arrives to the ground with an acceleration soft profile causing a null joint velocity reference at the time that the foot reaches the ground. Therefore, PZ_1 is achieved in the closed-loop system with the controller defined in (31) and additionally it must ensure that $\left[\dot{q}_1\ \dot{q}_2\ \dot{q}_3\ \dot{q}_4\right]^T$ (22) are zero in the surface S to kept null the error despite the foot-floor impact. If that so, it is possible through ref. [4] to represent the v_{hip} dynamics between successive impacts as a discrete system with the form:

$$z\,[k+1] = \rho_{\epsilon 1}\,(z\,[k]), \tag{36}$$

where $\rho_{\epsilon_1} = S \cap PZ_1 \cap Z \rightarrow S \cap PZ_1 \cap Z$ depends on $\epsilon_1 = \frac{k_s}{1+\sigma_{real}}$ from (32). As it is proven in (Theorem 2 in [4]), there exists an $\epsilon > 0$ such that for $\epsilon_1 > \epsilon$, $\left|\dot{\rho}_{\epsilon_1}\,(z\,[k])\right| < 1$ establishing the stability of the periodic orbit for the PHZD. On the other hand, we use the PHZD concept into the yaw turn in an analog way to how ref. [4] applies it to control $\tilde{y}_2$ forcing that $\tilde{y}_2$ remains invariant on the impact and therefore the continuous controller can be applied to the hybrid dynamics. For the yaw control, we define:

$$PZ_2 = \left\{ (\mathbf{x}, z) \in R^{4n+1} : \tilde{\mathbf{y}}_{\mathbf{3}}(\mathbf{q}) = \mathbf{0}, \dot{\tilde{\mathbf{y}}}_{\mathbf{3}} = \mathbf{0} \right\}. \tag{37}$$

The turn reference proposed in (24) holds condition (37), since $\dot{\tilde{\mathbf{y}}}_3$ does not change because at the moment of impact on the ground, the foot has a null yaw rate, due to the yaw reference is retained constant for a sufficiently long time such that $(\mathbf{q}, \dot{\mathbf{q}})$ belong to PZ_2, before that foot-floor impact.

4. Stability of the Delayed Bilateral Teleoperation System

4.1. Stability of delayed virtual system

To begin the stability analysis, a positive definite functional $V\,(t, \mathbf{x}) = V_1 + V_2 + V_3 + V_4 + V_5$, with $\mathbf{x} := \left[\mathbf{x_m}, \dot{\mathbf{x}}_\mathbf{m}, k_g\mathbf{x_m} - \boldsymbol{\eta}, \dot{\boldsymbol{\eta}}\right]$, is built to evaluate the evolution of a virtual system from a finite initial condition. The functional V is formed by:

$$V_1 = \frac{1}{2}\dot{\mathbf{x}}_\mathbf{m}^\mathbf{T}\mathbf{M_m}\,(\mathbf{x_m})\,\dot{\mathbf{x}}_\mathbf{m}, \tag{38}$$

$$V_2 = \frac{1}{2}\frac{k_m}{k_g}\left(k_g\mathbf{x_m} - \boldsymbol{\eta}\right)^\mathbf{T}\left(k_g\mathbf{x_m} - \boldsymbol{\eta}\right), \tag{39}$$

$$V_3 = \frac{1}{2}\kappa_m\mathbf{x_m}^\mathbf{T}\mathbf{x_m}, \tag{40}$$

$$V_4 = \frac{1}{2}\frac{k_m}{k_s k_g}\int_0^t \dot{\boldsymbol{\eta}}^\mathbf{T}\,(\xi)\,\mathbf{D}\dot{\boldsymbol{\eta}}\,(\xi)\,d\xi, \tag{41}$$

$$V_5 = \int_{-\bar{h}_2}^{0}\int_{t+\theta}^{t} \dot{\boldsymbol{\eta}}(\xi)^\mathbf{T}\dot{\boldsymbol{\eta}}\,(\xi)d\xi d\theta + \int_{-\bar{h}_1}^{0}\int_{t+\theta}^{t} \dot{\mathbf{x}}_\mathbf{m}(\xi)^\mathbf{T}\dot{\mathbf{x}}_\mathbf{m}\,(\xi)d\xi d\theta. \tag{42}$$

Following the procedure described in Appendix A, $\dot{V}$ along the trajectories of the closed- loop system, considering the virtual robot dynamics, master dynamics, time delay, and the human operator and environment forces, is bounded by:

https://doi.org/10.1017/S0263574720000636 Published online by Cambridge University Press

$$\begin{aligned}\dot{V} &\leq -\lambda_m \left\|\dot{\mathbf{x}}_m\right\|_2^2 - \lambda_s \left\|\dot{\boldsymbol{\eta}}\right\|_2^2 + \int_0^t \dot{\mathbf{x}}_m\left(\varepsilon\right)^T \mathbf{f}_{\mathbf{a_h}}\left(\varepsilon\right) d\varepsilon + \frac{k_m}{k_g k_s}\int_0^t \dot{\boldsymbol{\eta}}\left(\boldsymbol{\varepsilon}\right)^T \mathbf{f}_{\mathbf{v}}\left(\varepsilon\right) d\varepsilon \\ &\leq -\lambda_m \dot{\mathbf{x}}_{\mathbf{m}}^{\mathbf{T}} \dot{\mathbf{x}}_{\mathbf{m}} - \lambda_s \dot{\boldsymbol{\eta}}^{\mathbf{T}} \dot{\boldsymbol{\eta}} + \rho_m \left|\dot{\mathbf{x}}_{\mathbf{m}}\right| + \rho_s \left|\dot{\boldsymbol{\eta}}\right|,\end{aligned} \tag{43}$$

where

$$\begin{aligned}\lambda_m &= (\alpha_m + \alpha_h) - h_1 - \frac{k_m^2}{4} h_2, \\ \lambda_s &= \sigma_s \frac{k_m}{k_s k_g} - h_2 - \frac{k_m^2}{4} h_1,\end{aligned} \tag{44}$$

$$\begin{aligned}\rho_m &= \bar{f}_{ah}, \\ \rho_s &= \frac{k_m}{k_g k_s} \bar{f}_v.\end{aligned} \tag{45}$$

Result 1. If α_m and α_s are sufficiently high damping to fulfill λ_m, $\lambda_s > 0$ of (44), then we can point out from (43) that the variables $\dot{\mathbf{x}}_{\mathbf{m}}$, $\dot{\boldsymbol{\eta}} \in L_\infty$. As λ_m, λ_s be higher, rising the damping injected, then $\dot{\mathbf{x}}_{\mathbf{m}}$, $\dot{\boldsymbol{\eta}}$ will remain in a smaller origin-centered ball.

Result 2. Next, if (43) is integrated with respect to time, we get:

$$\begin{aligned}V\left(t, \mathbf{x}\right) - V\left(0\right) \leq -\lambda_m \left\|\dot{\mathbf{x}}_m\right\|_2^2 - \lambda_s \left\|\dot{\boldsymbol{\eta}}\right\|_2^2 + \int_0^t \dot{\mathbf{x}}_m\left(\varepsilon\right)^T \mathbf{f}_{\mathbf{a_h}}\left(\varepsilon\right) d\varepsilon \\ + \frac{k_m}{k_g k_s}\int_0^t \dot{\boldsymbol{\eta}}\left(\boldsymbol{\varepsilon}\right)^T \mathbf{f}_{\mathbf{v}}\left(\varepsilon\right) d\varepsilon.\end{aligned} \tag{46}$$

The terms $\int_0^t \dot{\mathbf{x}}_m\left(\varepsilon\right)^T \mathbf{f}_{\mathbf{a_h}}\left(\varepsilon\right) d\varepsilon$ and $\frac{k_m}{k_g k_s}\int_0^t \dot{\boldsymbol{\eta}}\left(\boldsymbol{\varepsilon}\right)^T \mathbf{f}_{\mathbf{v}}\left(\varepsilon\right) d\varepsilon$ are bounded $\mathbf{f}_{\mathbf{v}}, \mathbf{f}_{\mathbf{a_h}} \in L_2$ since (**Assumption 2**) and $\dot{\mathbf{x}}_{\mathbf{m}}$, $\dot{\boldsymbol{\eta}} \in L_\infty$ (**Result 1**). From (46), it is possible to get that $V(t)$ (function increasing respect to $\mathbf{x}$) is bounded for all t and therefore the state $\mathbf{x}$ is bounded, which implies that $\mathbf{x}_{\mathbf{m}}$, $\dot{\mathbf{x}}_{\mathbf{m}}$, $k_g \mathbf{x}_{\mathbf{m}} - \boldsymbol{\eta}$, $\boldsymbol{\eta}$, $\dot{\boldsymbol{\eta}} \in L_\infty$.

4.2. Stability of hybrid real system

Next, the convergence rate of the hybrid dynamics of v_{hip} is evaluated. First, from the explicit solution of the continuous dynamics of (32), the convergence rate c_3 can be found, see Definition 1,

$$c_3 = \frac{k_s}{1 + \sigma_{real}}. \tag{47}$$

On the other hand, the velocity's component v of the $\boldsymbol{\eta}$ vector is analyzed, where if $\mathbf{f}_s$ (14) is applied to the virtual bipedal robot (9), and considering (15), we have:

$$\dot{v} = c_{3virtual}\left(v_{ref} - v\right), \tag{48}$$

where $c_{3virtual} = \frac{k_s}{(\mathbf{D} + \sigma_s)}$ as it was proposed in ref. [19], it is possible to reach a stable exponentially hybrid system if the continuous part (32) is sufficiently rapid through c_3 (47) to hold the following condition:

$$\begin{aligned}c_1 - c_2 L_{\Delta x}^2 e^{-c_3 0.9 T^*} &> 0, \\ -\frac{1}{0.9T \ln\left(\frac{c_1}{c_2 L_{\Delta X}^2}\right)} &< c_3,\end{aligned} \tag{49}$$

where T is the period of the orbit O_z, L_{Δ_X} the Lipschitz constant for Δ_X that holds $\left\|\Delta_X\left(\mathbf{x}, z\right)\right\|^2 \leq L_{\Delta_X}^2 \left\|\mathbf{x}\right\|^2$, and c_1, c_2, c_3 depend on the continuous dynamics (32) like (3), (4) and (5). Therefore,

https://doi.org/10.1017/S0263574720000636 Published online by Cambridge University Press

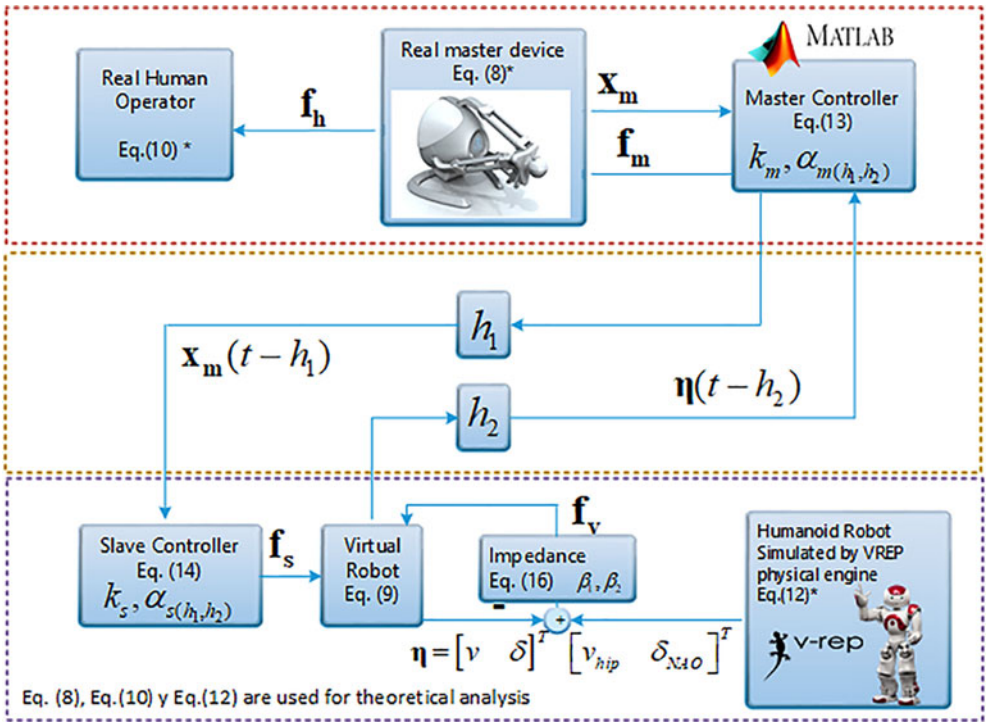

Fig. 4. Block diagram of the delayed bilateral teleoperation.

joining (47) and (49) we get:

$$\frac{k}{T} < \frac{k_s}{1+\sigma_{real}}, \tag{50}$$

where $k = -\frac{1}{0.9T} ln\left(\frac{c_1}{c_2 L_{\Delta_x}^2}\right)$. From (50), we propose a virtual continuous system whose response has a convergence rate that bounds the response of the hybrid dynamics of the robot speed. This concept allows linking (48) and (50), considering the virtual mass $\mathbf{D} = 1$, as follows:

$$\frac{k_s}{1+\sigma_{real}} - \frac{k}{T} > \frac{k_s}{(1+\sigma_s)}. \tag{51}$$

As a result we get the parameter k_s that depends on the time delay and walking cycle time, while the injected real damping σ_{real} is a function of σ_s which in turn depends on the time delay from (44). Thus, if the time delay increases, then the master damping as well as the virtual damping must be raised too to hold (43) and therefore an increment of the real damping injected to the bipedal robot is performed slowing thus the convergence rate ϵ_1 of the continuous part. This procedure can be applied while ϵ_1 be greater that a minimum bound ϵ.[4] It is important to remark that the time delay cannot be controlled, but the designer can online change k_s and T depending on the time delay.

5. Experimental Results

In this section, we present results of a test where a human operator drives a 3D simulated bipedal robot in order to verify that a delayed bilateral teleoperation of a bipedal robot can be achieved. The humanoid robot simulated in the Virtual Robot Experimentation Platform (VREP) 3D simulator is the NAO. The test performed consists of the teleoperator handling the NAO (simulated humanoid) from a hand controller of 2DOF with force feedback in order to obtain a forward movement driving its hip's velocity and turn control, despite the presence of time-varying delay while the humanoid robot follows the path remarked in red color. This delay has been modeled as a variable represented by a time-varying signal plus a filtered Gaussian noise (M_1 (t), M_2 (t)). The delays are $h_1 = (1.5 + 0.5\sin(2\pi 0.25t) + M_1(t))$ and $h_2 = (1.5 + M_2(t))$. The scheme used to perform the human in the loop simulations is presented in Fig. 4, where the equations that are used in each block

https://doi.org/10.1017/S0263574720000636 Published online by Cambridge University Press

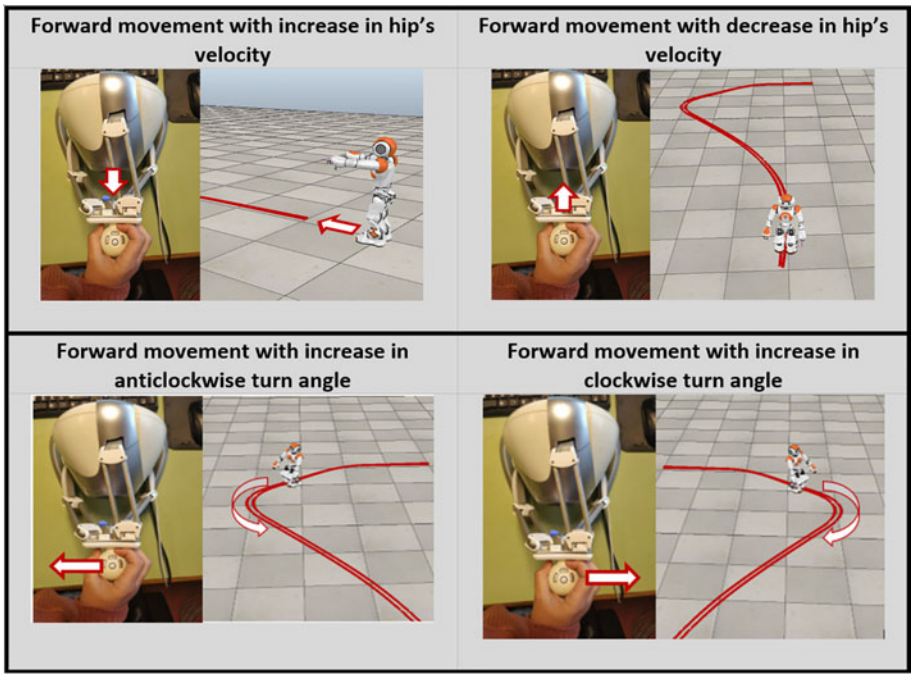

Fig. 5. Testing workspace (each square measures 50 cm side) and task to be perform.

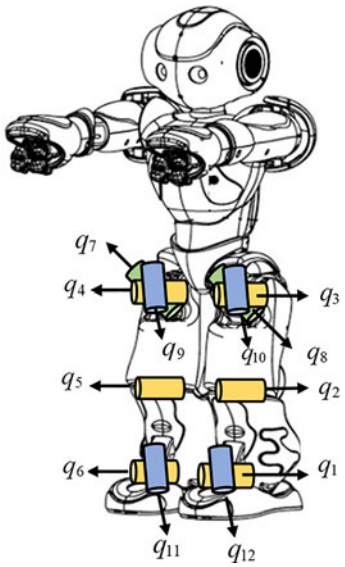

Fig. 6. Angles used in the 3D stable walk control.

and their respective control parameters are displayed. Figure 5 shows a sequence of images of one of the experiments developed, where the scenario and the execution of the test are displayed.

The control parameters k_m, k_g, β_1, and β_2 are calibrated in tests without delay, while α_m, σ_s, and k_s are coefficients of damping injected and proportional gain, depending on the time delay and walking cycle time, as it is proposed in Eqs. (44) and (51). The walking cycle is performed on the sagittal plane while turn control is applied to the 3D virtual NAO robot. Also, a lateral stability controller is performed to maintain lateral balance through the walking step, where the lateral tilt of the robot is measured and used to compute the left-right hip's roll and ankle's roll angles. Such controller is defined by: $q_9 = q_{10} = q_{11} = q_{12} = -K_{roll}\theta_{NAO}$, where $K_{roll} = 0.1$. Figure 6 shows all joints used in the simulated humanoid (NAO).

https://doi.org/10.1017/S0263574720000636 Published online by Cambridge University Press

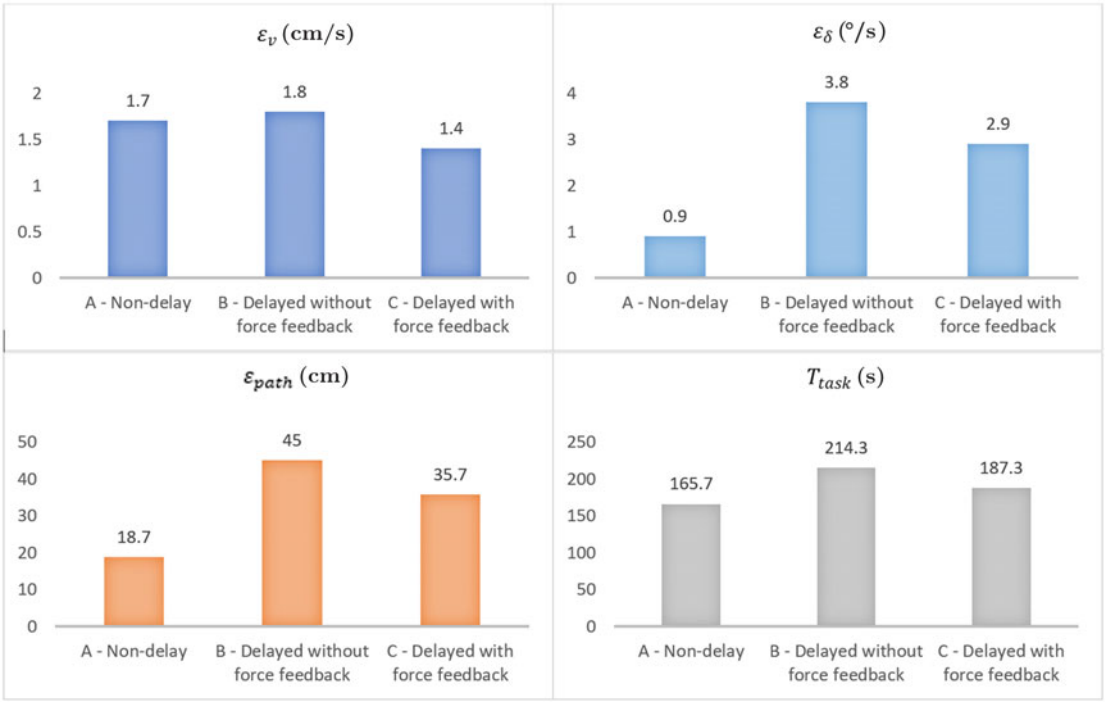

Fig. 7. Performance indexes of the tests.

Each experiment is repeated five times with one human operator, and the average values of syncronization error, path error, and time-to-complete the task are computed as follows to analyze the overall performance obtained in practice:

- Syncronization error, error between the position or reference speed (measured at the local site) and the position or speed of the slave robot (measured at the remote site), $\varepsilon_s = \begin{bmatrix} \varepsilon_v & \varepsilon_\delta \end{bmatrix}^T$, which measures both velocity and turning errors, and it is computed as follows:

$$\varepsilon_s = \frac{1}{n} \sum_{i=1}^{n} \frac{1}{t_{f_i}} \int_0^{t_{f_i}} \left| k_g \mathbf{x}_{\mathbf{m}_i}(t) - \boldsymbol{\eta}_i(t) \right| dt.$$

- Path error ε_{path}, error between the reference path and the path followed by the bipedal robot teleoperated by the human operator.
- Average time to complete the task T_{task} is defined by

$$T_{task} = \frac{1}{n} \sum_{i=1}^{n} t_{f_i},$$

where n is the quantity of tests made for the following cases : (A) non-delay, (B) delayed without force feedback, and (C) delayed with force feedback. Besides, t_{f_i} is the time consumed by the operator to complete the task in each test.

For case A, the proposed controller in Eqs. (13) and (14) has $\alpha_m = 0$, $\sigma_s = 0$, and $k_m = 0$; which means that there is no force feedback applied to the operator. The controller is calibrated in a similar way for case B. Finally, in case C, a force is fed back to the human operator using the following control parameters: $\alpha_m = 0.5$, $\sigma_s = 0.01$, and $k_m = \begin{bmatrix} 1 & 0 \\ 0 & 0.1 \end{bmatrix}$.

The results of the simulations for cases A, B, and C are shown in Fig. 7, and the experiments of cases A and C are shown in this video: https://youtu.be/gi80IfDccsM. It can be observed that as the time delay is higher, the turn angle error, the path error, and the time to complete the task are worse. When there is time delay, the indexes improve if force feedback is applied, since the human operator

https://doi.org/10.1017/S0263574720000636 Published online by Cambridge University Press

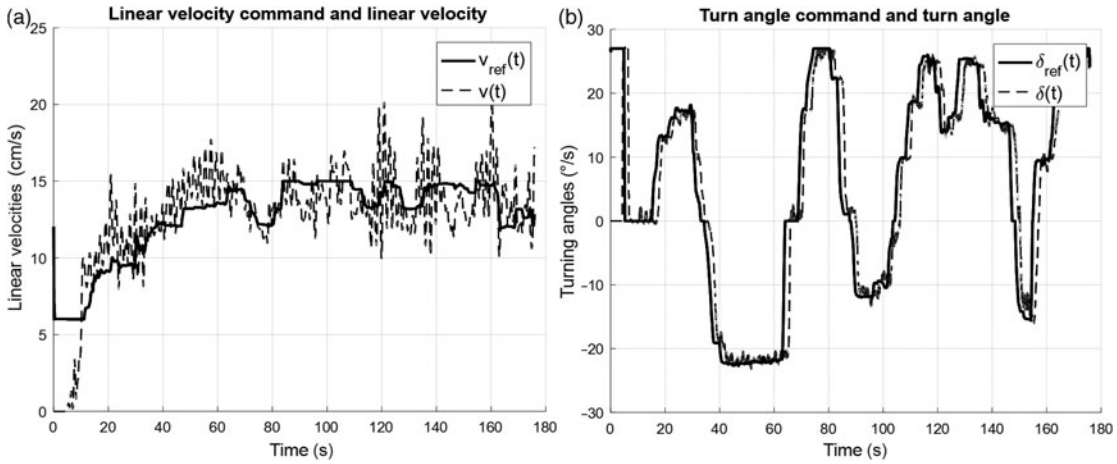

Fig. 8. (a) Robot linear velocity and reference from human operator. (b) Robot turn angle and command.

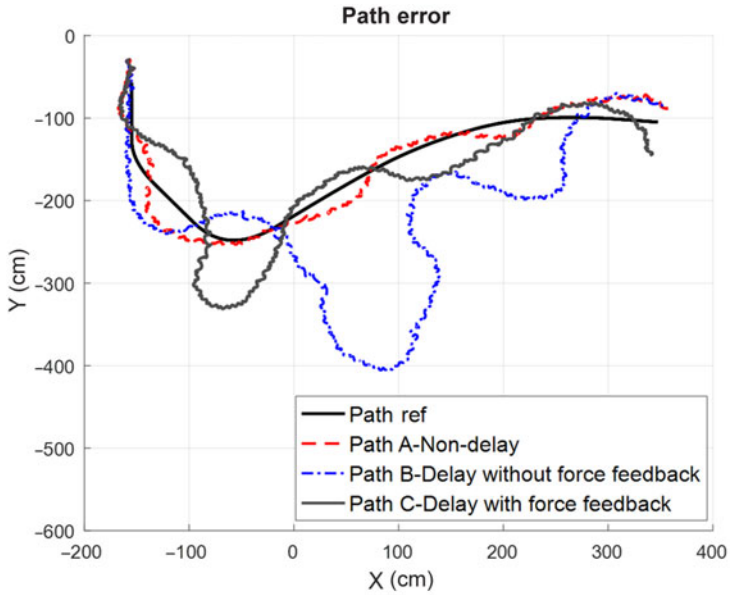

Fig. 9. Path error in the three schemes.

perception is enhanced, preventing rapid movements of the master and pressing the master toward a less synchronization error.

Using the proposed scheme (C), bounded synchronization errors are obtained despite the time-varying delay, which is shown in Fig. 8(a) and (b), which agrees with the theoretical result achieved in Eq. (46). Besides, it is important to remark that in practice, the proposed control scheme allows to get a path following more close to the non-delayed case A, as shown in Fig. 9.

Furthermore, from Figs. 10, 11, and 12, the angles of the real and reference trajectories of the bipedal robot in joint coordinates for case C are shown, during an arbitrary time interval of 50 to 65 [s], where the joint trajectories change according to the speed reference. Figure 10 shows the trajectory of the left and right ankle's angles. Figure 11 shows the left and right knee's angle which in every cycle change between oscillation-leg and stand-leg, while Fig. 12 shows the left and right hip's angles. The proposed controller maintain bounded joint errors.

The contribution of this paper is the shared control scheme that includes a stable control of bilateral teleoperation of a humanoid robot with time delay. The human operator can handle the speed and turn of a bipedal robot while also receives a force feedback that helps him to drive the robot remotely. This teleoperated control loop is integrated with an automatic control of balance of the torso to get a walking keeping lateral and frontal equilibrium.

https://doi.org/10.1017/S0263574720000636 Published online by Cambridge University Press

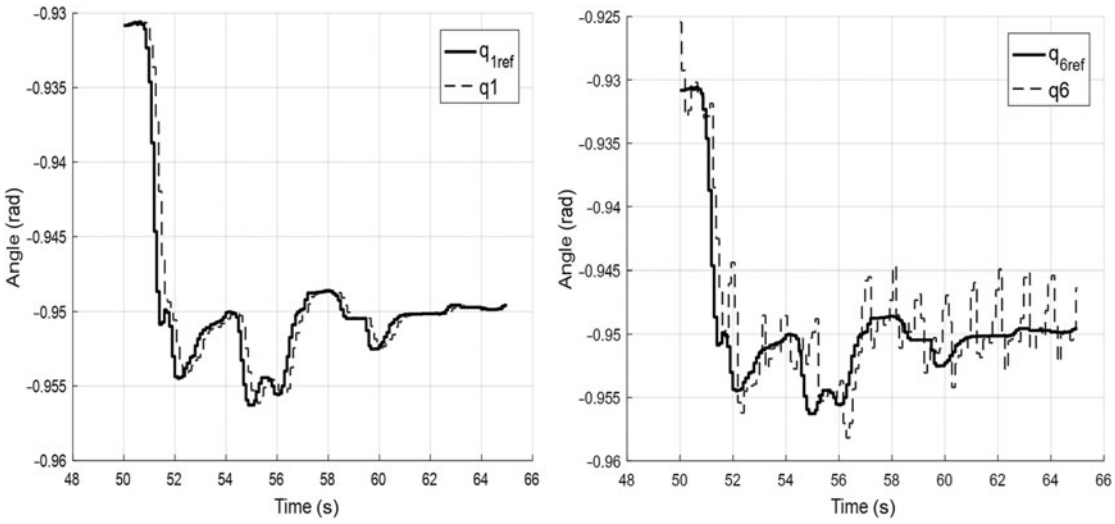

Fig. 10. Trajectories of the left-right ankle.

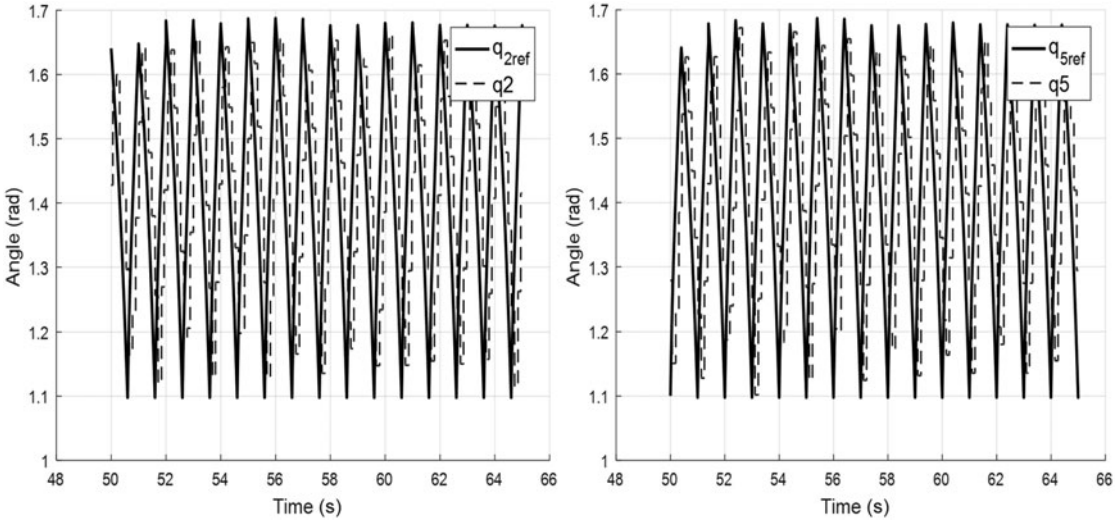

Fig. 11. Trajectories of the left-right knee.

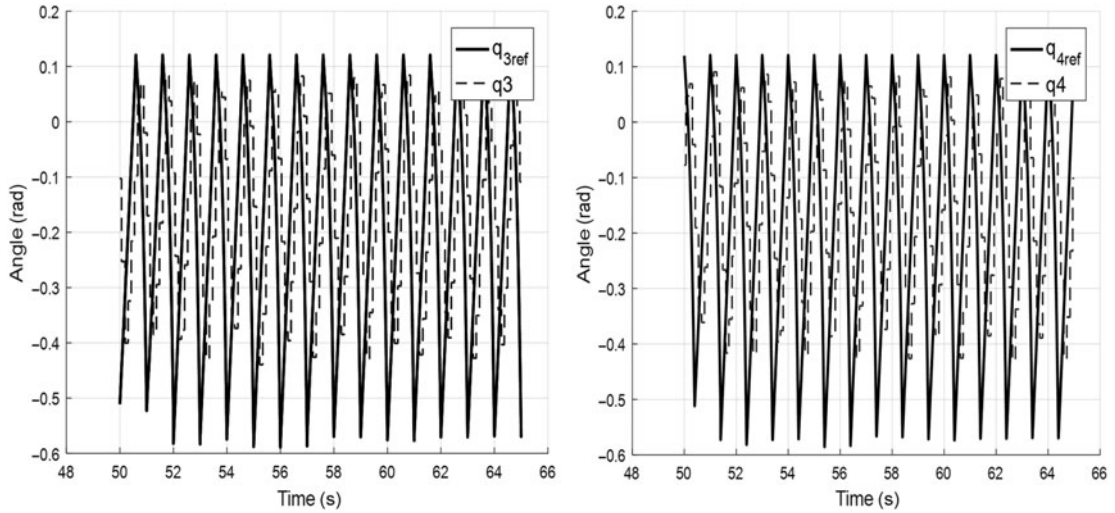

Fig. 12. Trajectories of the left-right hip.

https://doi.org/10.1017/S0263574720000636 Published online by Cambridge University Press

6. Conclusions

In this paper, a shared control scheme for delayed bilateral teleoperation of a biped robot has been proposed. The strategy uses a coupling impedance to link the bipedal robot with the virtual robot. The teleoperator drives the system from a 2D hand controller with force feedback. The joint angles are modulated by the speed and turn references generated online for the human operator, and they are based on human-inspired foot trajectories on the sagittal plane and a PHZD for the turn. The force feedback allows avoiding sudden motions of the master device, but it is gradually released (injecting lower viscous friction) as the time delay is smaller while also the human operator hand is pushed to directions of lower synchronism error. Besides, another quantitative metrics is analyzed which indirectly measures the system performance and allows us to know which test has the lowest error when time delay is applied. Finally, a 3D NAO-simulated robot was satisfactorily teleoperated in bilateral way despite a time-varying delay.

References

1. E. R. Westervelt, J. W. Grizzle, C. Chevallereau, J. H. Choi and B. Morris, *Feedback Control of Dynamic Bipedal Robot Locomotion* (CRC Press, Boca Raton, FL, 2007).
2. C.-L. Shih, J. W. Grizzle and C. Chevallereau, "From stable walking to steering of a 3D bipedal robot with passive point feet," *Robotica* **30**(7), 1119–1130 (2012).
3. F. Plestan, J. W. Grizzle, E. R. Westervelt and G. Abba, "Stable walking of a 7-DOF biped robot," *IEEE Trans. Robot. Autom.* **19**(4), 653–668 (2003).
4. A. D. Ames, "Human-inspired control of bipedal walking robots," *IEEE Trans. Autom. Contr.* **59**(5), 1115–1130 (2014).
5. J. P. Ferreira, T. G. Amaral, V. F. Pires, M. M. Crisostomo and P. Coimbra, "A Neural-Fuzzy Walking Control of an Autonomous Biped Robot," *Proceedings World Automation Congress*, Seville, Spain (2004) pp. 253–258.
6. J. H. Park, "Fuzzy-logic zero-moment-point trajectory generation for reduced trunk motions of biped robots," *Fuzzy Sets Syst.* **134**(1), 189–203 (2003).
7. C. Chevallereau, J. W. Grizzle and C.-L. Shih, "Asymptotically stable walking of a five-link underactuated 3-D bipedal robot," *IEEE Trans. Robot.* **25**(1), 37–50 (2009).
8. R. D. Gregg and M. W. Spong, "Bringing the Compass-Gait Bipedal Walker to Three Dimensions," *Proceedings of the International Conference on Intelligent Robots and Systems*, St. Louis, MO, USA (2009) pp. 4469–4474.
9. R. D. Gregg and M. W. Spong, "Reduction-Based Control with Application to Three-Dimensional Bipedal Walking Robots," *Proceedings of the 2008 American Control Conference*, Seattle, WA, USA (2008) pp. 880–887.
10. K. Miura, S. Nakaoka, M. Morisawa, F. Kanehiro, K. Harada and S. Kajita, "Analysis on a Friction Based "Twirl" for Biped Robots," *Proceedings of the IEEE International Conference on Robotics and Automation*, Anchorage, AK, USA (2010) pp. 4249–4255.
11. H. Shahbazi, K. Jamshidi and A. H. Monadjemi, "Curvilinear bipedal walk learning in nao humanoid robot using a CPG based policy gradient method," *Appl. Mech. Mater.* **110–116**, 5161–5166 (2012).
12. E. Slawiñski, V. A. Mut, P. Fiorini and L. R. Salinas, "Quantitative absolute transparency for bilateral teleoperation of mobile robots," *IEEE Trans. Syst. Man Cybern. A Syst. Hum.* **42**(2), 430–442 (2012).
13. L. Peternel and J. Babic, "Learning of compliant human-robot interaction using full-body haptic interface," *Adv. Robot.* **27**(13), 1003–1012 (2013).
14. A. Brygo, I. Sarakoglou, N. Garcia-Hernandez, and N. Tsagarakis, "Humanoid Robot Teleoperation with Vibrotactile Based Balancing Feedback," **In:** *Haptics: Neuroscience, Devices, Modeling, and Applications* (M. Auvray and C. Duriez, eds.), LNCS, vol. 8619 (Springer, Berlin, Heidelberg, 2014) pp. 266–275.
15. J. Ramos and S. Kim, "Humanoid dynamic synchronization through whole-body bilateral feedback teleoperation," *IEEE Trans. Robot.* **34**(4), 953–965 (2018).
16. B. Wang and C. Yang and Q. Xie, "Human-Machine Interfaces Based on EMG and Kinect Applied to Teleoperation of a Mobile Humanoid Robot," *Proceedings of the 10th World Congress on Intelligent Control and Automation*, Beijing, China (2012) pp. 3903–3908.
17. S. Mukherjee, D. Paramkusam and S. K. Dwivedy, "Inverse Kinematics of a NAO Humanoid Robot Using Kinect to Track and Imitate Human Motion," *Proceedings of the International Conference on Robotics, Automation, Control and Embedded Systems (RACE)*, Chennai, India (2015) pp. 1–7.
18. C. Hua and X. P. Liu, "Delay-dependent stability criteria of teleoperation systems with asymmetric time-varying delays," *IEEE Trans. Robot.* **26**(5), 925–932 (2010).
19. A. Ames, K. Galloway, K. Sreenath and J. W. Grizzle, "Rapidly exponentially stabilizing control Lyapunov functions and hybrid zero dynamics," *IEEE Trans. Autom. Contr.* **59**(4), 876–891 (2014).
20. N. Karbasizadeh, M. Zarei, A. Aflakian, M. Tale Masouleh and A. Kalhor, "Experimental dynamic identification and model feed-forward control of Novint Falcon haptic device," *Mechatronics* **51**, 19–30 (2018).
21. E. Nuño, R. Ortega, N. Barabanov and L. Basañez, "A globally stable PD ccontroller for bilateral teleoperators," *IEEE Trans. Robot.* **24**(3), 753–758 (2008).

https://doi.org/10.1017/S0263574720000636 Published online by Cambridge University Press

22. H. Li, L. Zhang and K. Kawashima, "Operator dynamics for stability condition in haptic and teleoperation system: A survey," *Int. J. Med. Robot. Comput. Assist. Surg.* **14**(2), 1–10 (2018).
23. E. Nuño, L. Basañez and R. Ortega,"Passivity-based control for bilateral teleoperation: A tutorial," *Automatica* **47**(3), 485–495 (2011).
24. E. Slawiñski, V. Mut and D. Santiago,"PD-like controller for delayed bilateral teleoperation of wheeled robots," *Int. J. Contr.* **89**(8), 1622–1631 (2016).
25. Dongjun Lee, O. Martinez-Palafox and M. W. Spong, "Bilateral Teleoperation of a Wheeled Mobile Robot Over Delayed Communication Network," *Proceedings 2006 IEEE International Conference on Robotics and Automation*, Orlando, FL, USA (2006) pp. 3298–3303.
26. L. Salinas, D. Santiago, E. Slawiñski, V. A. Mut, D. Chavez, P. Leica and O. Camacho,"P+d plus sliding mode control for bilateral teleoperation of a mobile robot," *Int. J. Contr. Autom. Syst.* **16**(4), 1927–1937 (2018).
27. C. Vaughan, B. Davis and J. O'Connor, *Dynamics of Human Gait* (Human Kinetics Publishers, Champaign, IL, 1992).
28. Y. Ivanenko, R. Grasso, V. Macellari and F. Lacquaniti, "Control of foot trajectory in human locomotion: Role of ground contact forces in simulated reduced gravity," *J. Neurophysiol.* **87**(6), 3070–3089 (2002).
29. M. W. Spong, S. Hutchinson and M. Vidyasagar, *Robot Modeling and Control* (John Wiley & Sons, Inc., Hoboken, NJ, 2005).

A. Appendix

Given the functional $V(t, \mathbf{x}) = V_1 + V_2 + V_3 + V_4 + V_5$ represented by (38), (39), (40), (41), and (42), its derivative along the system trajectories will be obtained.

First, $\dot{V}_1$ of (38), including the master dynamics (8), and taking into account properties 1 and 2, is accomplished as follows:

$$\begin{aligned}\dot{V}_1 &= \frac{1}{2}\dot{\mathbf{x}}_\mathbf{m}^\mathbf{T}\dot{\mathbf{M}}_\mathbf{m}\dot{\mathbf{x}}_\mathbf{m} + \dot{\mathbf{x}}_\mathbf{m}^\mathbf{T}\mathbf{M}_\mathbf{m}\ddot{\mathbf{x}}_\mathbf{m} \\ &= \frac{1}{2}\dot{\mathbf{x}}_\mathbf{m}^\mathbf{T}\dot{\mathbf{M}}_\mathbf{m}\dot{\mathbf{x}}_\mathbf{m} + \dot{\mathbf{x}}_\mathbf{m}^\mathbf{T}\mathbf{M}_\mathbf{m}\mathbf{M}_\mathbf{m}^{-\mathbf{1}}\left(\mathbf{f}_\mathbf{m} + \mathbf{f}_\mathbf{h} - \mathbf{g}\left(\mathbf{x}_\mathbf{m}\right) - \mathbf{C}_\mathbf{m}\dot{\mathbf{x}}_\mathbf{m}\right) \\ &= \dot{\mathbf{x}}_\mathbf{m}^\mathbf{T}\left(\mathbf{f}_\mathbf{m} + \mathbf{f}_\mathbf{h} - \mathbf{g}_\mathbf{m}\left(\mathbf{x}_\mathbf{m}\right)\right).\end{aligned} \tag{A1}$$

If the control action $\mathbf{f_m}$ (13) and the human force $\mathbf{f_h}$ (10) are included in (A1), and then grouping terms by convenience considering also (15), it yields:

$$\begin{aligned}\dot{V}_1 &= -\kappa_m\dot{\mathbf{x}}_\mathbf{m}^\mathbf{T}\mathbf{x}_\mathbf{m} - \alpha_m\dot{\mathbf{x}}_\mathbf{m}^\mathbf{T}\dot{\mathbf{x}}_\mathbf{m} - k_m\dot{\mathbf{x}}_\mathbf{m}^\mathbf{T}\left(k_g\mathbf{x}_\mathbf{m} - \boldsymbol{\eta}\left(t - h_2\right)\right) - \alpha_h\dot{\mathbf{x}}_\mathbf{m}^\mathbf{T}\dot{\mathbf{x}}_\mathbf{m} + \dot{\mathbf{x}}_\mathbf{m}^\mathbf{T}\mathbf{f}_{\mathbf{a_h}} \\ &\leq -\kappa_m\dot{\mathbf{x}}_\mathbf{m}^\mathbf{T}\mathbf{x}_\mathbf{m} - \left(\alpha_m + \alpha_h\right)\dot{\mathbf{x}}_\mathbf{m}^\mathbf{T}\dot{\mathbf{x}}_\mathbf{m} - k_m\dot{\mathbf{x}}_\mathbf{m}^\mathbf{T}\left(k_g\mathbf{x}_\mathbf{m} - \boldsymbol{\eta}\right) \\ &\quad - k_m\dot{\mathbf{x}}_\mathbf{m}^\mathbf{T}\int_{t-h_2}^{t}\dot{\boldsymbol{\eta}}\left(\xi\right)d\xi + \dot{\mathbf{x}}_\mathbf{m}^\mathbf{T}\mathbf{f}_{\mathbf{a_h}}.\end{aligned} \tag{A2}$$

Next, $\dot{V}_2$ is attained from (39) as:

$$\dot{V}_2 = \frac{k_m}{k_g}\left(k_g\mathbf{x}_\mathbf{m} - \boldsymbol{\eta}\right)^\mathbf{T}\left(k_g\dot{\mathbf{x}}_m - \dot{\boldsymbol{\eta}}\right) = k_m\left(k_g\mathbf{x}_\mathbf{m} - \boldsymbol{\eta}\right)^\mathbf{T}\dot{\mathbf{x}}_m - \frac{k_m}{k_g}\left(k_g\mathbf{x}_\mathbf{m} - \boldsymbol{\eta}\right)^\mathbf{T}\dot{\boldsymbol{\eta}}. \tag{A3}$$

Now, $\dot{V}_3$ is computed from (40):

$$\dot{V}_3 = \kappa_m\mathbf{x}_\mathbf{m}^\mathbf{T}\dot{\mathbf{x}}_\mathbf{m}. \tag{A4}$$

Besides, $\dot{V}_4$ from (41) including the virtual robot dynamics (9) as well as the control action $\mathbf{f}_s$ (14), is given by:

$$\begin{aligned}\dot{V}_4 &= \frac{k_m}{k_sk_g}\boldsymbol{\eta}^\mathbf{T}\mathbf{D}\dot{\boldsymbol{\eta}} = \frac{k_m}{k_sk_g}\dot{\boldsymbol{\eta}}^\mathbf{T}\mathbf{D}\mathbf{D}^{-\mathbf{1}}\left[\mathbf{f_s} - \mathbf{f_e}\right] \\ &= \frac{k_m}{k_sk_g}\dot{\boldsymbol{\eta}}^\mathbf{T}\left[k_s\left(k_g\mathbf{x}_\mathbf{m}\left(t - h_1\right) - \boldsymbol{\eta}\right) - \sigma_s\Psi - \mathbf{f_v}\right],\end{aligned} \tag{A5}$$

next, if the human force $\mathbf{f_h}$ (10) is inserted into (A5), considering in there (15), the below expression is reached:

$$\dot{V}_4 \leq \frac{k_m}{k_g}\dot{\boldsymbol{\eta}}^\mathbf{T}\left(k_g\mathbf{x}_\mathbf{m} - \boldsymbol{\eta}\right) - k_m\dot{\boldsymbol{\eta}}^\mathbf{T}\int_{t-h_1}^{t}\dot{\mathbf{x}}_m\left(\xi\right)d\xi - \frac{\sigma_sk_m}{k_sk_g}\dot{\boldsymbol{\eta}}^\mathbf{T}\dot{\boldsymbol{\eta}} - \frac{k_m}{k_sk_g}\dot{\boldsymbol{\eta}}^\mathbf{T}\mathbf{f_v}. \tag{A6}$$

https://doi.org/10.1017/S0263574720000636 Published online by Cambridge University Press

The stability analysis is difficult because there are terms with delayed variables in (A2) and (A6). For solving this, V_5 (42) has been proposed whose derivative considering Assumption 1, is obtained by:

$$\begin{aligned}\dot{V}_5 &= \bar{h}_2\dot{\boldsymbol{\eta}}^{\mathbf{T}}\dot{\boldsymbol{\eta}} - \int_{t-\bar{h}_2}^{t}\dot{\boldsymbol{\eta}}^{\mathbf{T}}(\xi)\,\dot{\eta}(\xi)\,d\xi + \bar{h_1}\dot{\mathbf{x}}_{\mathbf{m}}^{\mathbf{T}}\dot{\mathbf{x}}_{\mathbf{m}} - \int_{t-\bar{h_1}}^{t}\dot{\mathbf{x}}_{\mathbf{m}}^{\mathbf{T}}(\xi)\,\dot{\mathbf{x}}_{\mathbf{m}}(\xi)\,d\xi \\ &\leq \bar{h}_2\dot{\boldsymbol{\eta}}^{\mathbf{T}}\dot{\boldsymbol{\eta}} - \int_{t-h_2}^{t}\dot{\boldsymbol{\eta}}^{\mathbf{T}}(\xi)\,\dot{\eta}(\xi)\,d\xi + \bar{h_1}\dot{\mathbf{x}}_{\mathbf{m}}^{\mathbf{T}}\dot{\mathbf{x}}_{\mathbf{m}} - \int_{t-h_1}^{t}\dot{\mathbf{x}}_{\mathbf{m}}^{\mathbf{T}}(\xi)\,\dot{\mathbf{x}}_{\mathbf{m}}(\xi)\,d\xi,\end{aligned} \tag{A7}$$

the terms with integrals of (A7) can be linked with others of (A2) and (A6) by using Lemma 1 (1), yielding the relations

$$-k_m\dot{\mathbf{x}}_{\mathbf{m}}^{\mathbf{T}}\int_{t-h_2}^{t}\dot{\boldsymbol{\eta}}(\xi)d\xi - \int_{t-h_2}^{t}\dot{\boldsymbol{\eta}}^{\mathbf{T}}(\xi)\dot{\boldsymbol{\eta}}(\xi)d\xi \leq \frac{1}{4}h_2k_m^2\dot{\mathbf{x}}_{\mathbf{m}}^{\mathbf{T}}\dot{\mathbf{x}}_{\mathbf{m}}, \tag{A8}$$

$$-k_m\dot{\boldsymbol{\eta}}^{\mathbf{T}}\int_{t-h_1}^{t}\dot{\mathbf{x}}_{\mathbf{m}}(\xi)\,d\xi - \int_{t-h_1}^{t}\dot{\mathbf{x}}_{\mathbf{m}}^{\mathbf{T}}(\xi)\,\dot{\mathbf{x}}_{\mathbf{m}}(\xi)\,d\xi \leq \frac{1}{4}h_1k_m^2\dot{\boldsymbol{\eta}}^{T}\dot{\boldsymbol{\eta}}. \tag{A9}$$

Finally, $\dot{V}$ can be built joining Equations from (A2) to (A7), considering the relations given by (A8) and (A9) to avoid terms with integrals, and cancelling all opposing terms, as follows:

$$\begin{aligned}\dot{V} &= \dot{V}_1 + \dot{V}_2 + \dot{V}_3 + \dot{V}_4 + \dot{V}_5 \\ &\leq \dot{\mathbf{x}}_{\mathbf{m}}^{\mathbf{T}}\left[-(\alpha m + \alpha_h)\,\mathbf{I} + h_1\mathbf{I} + \frac{k_m^2}{4}h_2\mathbf{I}\right]\dot{\mathbf{x}}_{\mathbf{m}} + \dot{\boldsymbol{\eta}}^{\mathbf{T}}\left[-\sigma_s\frac{k_m}{k_sk_g}\mathbf{I} + h_2\mathbf{I} + \frac{k_m^2}{4}h_1\mathbf{I}\right]\dot{\boldsymbol{\eta}} \\ &\quad + \bar{f}_{a_h}\left|\dot{\mathbf{x}}_{\mathbf{m}}\right| + \frac{k_m}{k_sk_g}\bar{f}_v\left|\dot{\boldsymbol{\eta}}\right|.\end{aligned} \tag{A10}$$

The result achieved in (A10) is used to complete the stability proof and convergence analysis of the motion error between master position and speed-turn of the bipedal robot.

https://doi.org/10.1017/S0263574720000636 Published online by Cambridge University Press